Supplemental Material for "Exact Conditions for Ensemble Density Functional Theory"

Thais R. Scott,[1] John Kozlowski,[1] Steven Crisostomo,[2] Aurora Pribram-Jones,[3] and Kieron Burke[1,2]

[1]*Department of Chemistry, University of California, Irvine, CA 92697*
[2]*Department of Physics & Astronomy, University of California, Irvine, CA 92697*
[3]*Department of Chemistry, University of California, Merced, CA 95343*

(Dated: July 4, 2023)

Below we list the analytical expressions defining the Hubbard dimer bi-ensemble, and plot various weight-dependent quantities of interest. In all plots we set $t = 1/2$.

CONTENTS

1. EXACT SOLUTION

We begin with the analytic solutions of the Hubbard dimer that were used to create a bi-ensemble of the ground and first-excited singlet states. Solving the dimer Hamiltonian (Eq. 26), one obtains the energies:

$$E_i = \frac{2U}{3} + \frac{2r}{3}\cos\left[\theta + \frac{2\pi(i+1)}{3}\right], \qquad i = 0, 1. \tag{S.1}$$

Here we have defined

$$r = \sqrt{3\left(4t^2 + \Delta v^2\right) + U^2}, \qquad \cos(3\theta) = \frac{9U\left(\Delta v^2 - 2t^2\right) - U^3}{r^3},$$

where t represents the hopping parameter, U the on-site electrostatic self-repulsion, and $\Delta v = v_2 - v_1$ the on-site potential difference. Furthermore, the wavefunction of each state may be written as

$$|\Psi_i\rangle = \alpha_i\left(|12\rangle + |21\rangle\right) + \beta_i^+ |11\rangle + \beta_i^- |22\rangle, \tag{S.2}$$

with coefficients:

$$\alpha_i = \frac{2t\left(E_i - U\right)}{c_i E_i}, \qquad \beta_i^{\pm} = \frac{U - E_i \pm \Delta v}{c_i},$$

$$c_i = \sqrt{2\left[\Delta v^2 + \left(E_i - U\right)^2\left(1 + 4t^2/E_i^2\right)\right]}.$$

Here $|ij\rangle$ represents a state in which an electron is present at sites i and j. These analytical expressions (both of the energy and wavefunction) may also be found in the appendices of References 1 and 2.

1.1. Densities

We use the same bi-ensemble as described in the main text; the two lowest lying singlet states in the Hubbard dimer. The density of each state is trivially $\Delta n_i = 2[(\beta_i^-)^2 - (\beta_i^+)^2]$, meaning that the ensemble density is

$$\Delta n_w = 2\overline{w}\left[(\beta_0^-)^2 - (\beta_0^+)^2\right] + 2w\left[(\beta_1^-)^2 - (\beta_1^+)^2\right], \tag{S.3}$$

where $\overline{w} = 1 - w$. Plots of this difference are included below in Fig. S1 for three interaction strengths, $U = 0$, 1, & 5.

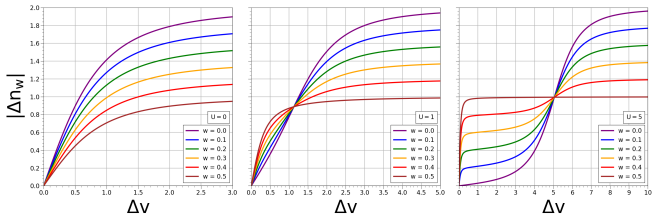

FIG. S1. Absolute value of the density of the Hubbard dimer bi-ensemble, plotted for various weight values as a function of Δv. Here we set $U = 0$ (left), $U = 1$ (center), and $U = 5$ (right).

Analyzing this figure, it is clear that there are vast differences in the behavior of Δn_w with respect to the value of U, illustrating the importance of developing weight-dependent approximations for electronic correlation. Two characteristics are present in all plots of Δn_w, these being an adherence to the symmetric limit ($\Delta v = \Delta n_w = 0$) and a maximum value constraint imposed by the representability condition $|\Delta n_w| \leq 2\overline{w}$, which each curve approaches as $\Delta v \to \infty$.

As predicted by EDFT (eq X), the density is linear in w. For sufficiently large U, there exists a value of Δv at which the initial slope of the first excited state density difference is negative, but it always becomes positive for sufficiently large Δv. Thus there is a specific value of Δv at which the first excited state density vanishes, and all curves meet at that point, independent of w. This point tends to $\Delta v = U$ as U becomes large.

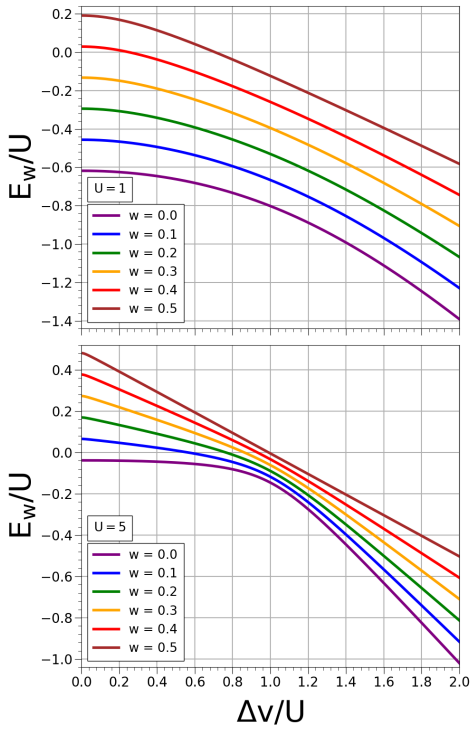

FIG. S2. Total energy of the Hubbard dimer bi-ensemble plotted as a function of Δv for various w values. Here we set $U = 1$ (top) and $U = 5$ (bottom).

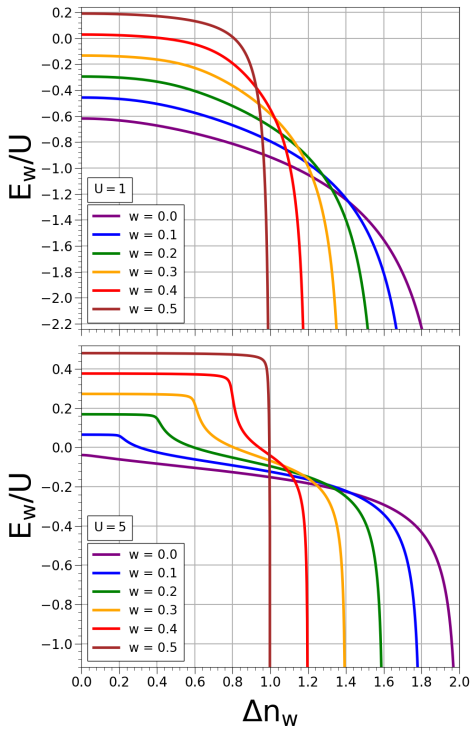

FIG. S3. Total energy of the Hubbard dimer bi-ensemble plotted as a function of Δn_w for various w values. Here we set $U = 1$ (top) and $U = 5$ (bottom).

For finite values of U, a trend in curve steepness with respect to the weight is evident for small Δv; the steepness of each curve is directly proportional to the value of w, signifying that ensembles with larger w values approach their maximum value more quickly. The severity of steepness increases drastically as U is increased, as shown by the behavior of the $U = 5$ curves as $\Delta v \to 0$. Here, the densities increase rapidly to $|\Delta n_w| \approx 2w$, becoming nearly perfectly anti-symmetric around $\Delta v = U$, with a very sharp dive to 0 for very small Δv.It also appears that all Δn_w curves approach the same value at $\Delta v \approx U$ as $U \to \infty$. As $U \to \infty$ the density forms a step function, flipping from $2w$ to $2\overline{w}$ at $\Delta v = U$ (see Fig. S13).

1.2. Total Energies

In this section we depict plots of the total bi-ensemble energy, E_w, defined as the weighted sum of Eq. 28. Here we choose to depict two interaction strengths ($U = 1$ and $U = 5$), plotting both as a function of Δv and Δn_w below. We make use of the derivation put forth by Deur *et al.* [1] to define:

$$T_{s,w} = -2t\sqrt{\overline{w}^2 - \Delta n_w^2/4} \tag{S.4}$$

$$E_{Hx,w} = \frac{U}{2}\left(1 + w - \frac{(3w-1)}{\overline{w}^2}\frac{\Delta n_w^2}{4}\right). \tag{S.5}$$

The correlation energies are then found by using the exact expressions:

$$T_{c,w} = T_w - T_{s,w}, \tag{S.6}$$

$$U_{c,w} = V_{\text{ee},w} - E_{Hx,w}, \tag{S.7}$$

$$E_{c,w} = T_{c,w} + U_{c,w}. \tag{S.8}$$

For fixed Δv, Fig. S2 illustrates that E_w is correctly linear in w. The curves are rather boring for $U = 1$, but develop a pinch around $\Delta v = U$ as U grows larger (see Sec X). However, Fig. S3 shows that, as a functional of Δn, the curves are no longer linear in w. They are not even monotonic. Moreover as $\Delta n_w \to 2\overline{w}$, $E_w \to -\infty$, ensuring the curves cross. There exists interesting behavior as U is increased, with E_w becoming ever more slowly varying with density for $\Delta n_w < 2w$. This behavior may be explained through the relationship between Δn_w and Δv shown in the right panel of Fig. S1, where there is drastic change in Δn_w for $\Delta v \approx 0$.

We also examine the properties of the Hubbard dimer equivalent of the universal part of the density functional, $F_w = E_w - \Delta v \Delta n_w/2$, plotting again as a function of Δv and Δn_w in Figs. S4 and S5 respectively. In Fig. S4, one can see that F_w is linear with respect to bi-ensemble weight when plotted as a function of Δv. This characteristic is not present in Fig. S5, where monotonicity is broken as

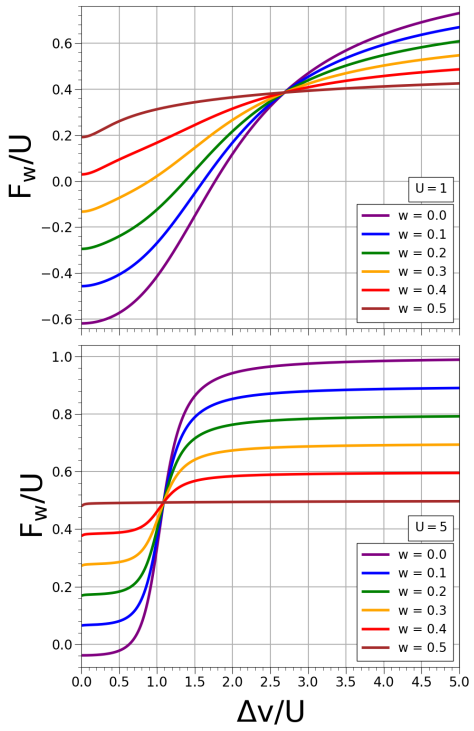

FIG. S4. F_w/U of the Hubbard dimer bi-ensemble plotted as a function of Δv for various w values. Here we set $U = 1$ (top) and $U = 5$ (bottom).

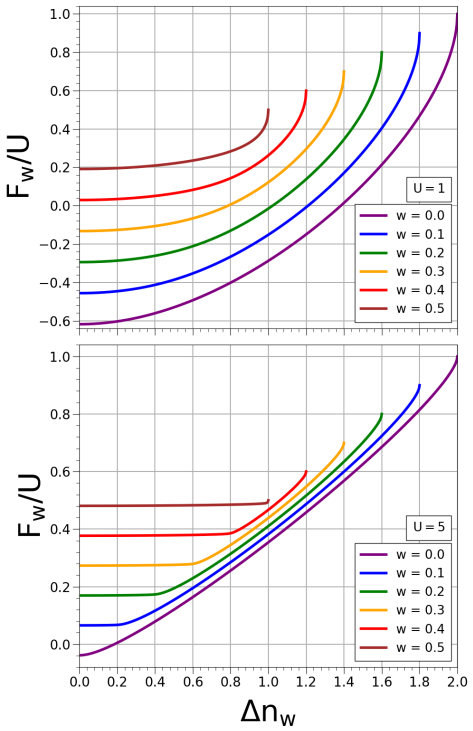

FIG. S5. F_w/U of the Hubbard dimer bi-ensemble plotted as a function of Δn_w for various w values. Here we set $U = 1$ (top) and $U = 5$ (bottom).

$\Delta n_w \to 2\overline{w}$. Furthermore, as U is increased, one can see the appearance of regimes around $\Delta n_w = 2w$, with F_w being nearly independent of Δn_w for $\Delta n_w < 2w$ and linearly increasing as $\Delta n_w > 2w$. Additionally, the curves depicting F_w tend to flatten as w increases.

In contrast, we plot $E_{\mathrm{HXC},w}$ in Fig. S6 and see it is non-monotonic in w. The curvature of $E_{\mathrm{HXC},w}$ changes from convex to concave as the weight is increased and the $E_{\mathrm{HXC},w}$ curves cross each other at various points; with the most noticeable crossings happening at $U = 1$. However, the curves cross at all the values of U plotted.

We conclude that curves become non-monotonic when plotted as a functional of the density instead of the potential, as the curves of Fig. S1 are definitely not monotonic.

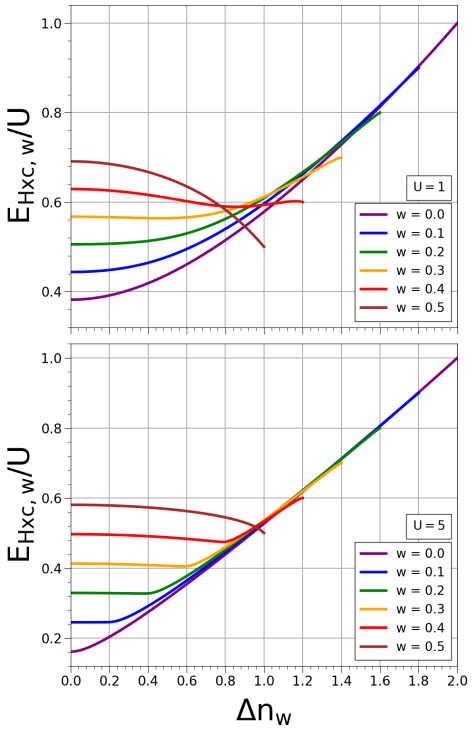

FIG. S6. $E_{\mathrm{HXC},w}/U$ of the Hubbard dimer bi-ensemble plotted as a function of Δn_w for various w values. Here we set $U = 1$ (top) and $U = 5$ (bottom).

1.3. Correlation Inequalities

In this section we depict the correlation inequalities (Eq. 21), showing more cases of Fig. 2 of the main text. We highlight in Fig. S7 the definite signs of the correlation energy and its components. This validates results initially introduced by Pribram-Jones *et al.* [3]

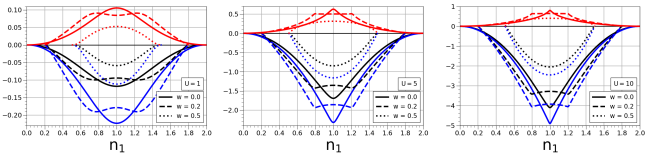

FIG. S7. Variation of the potential (blue), kinetic (red), and total (black) correlation energies in the Hubbard dimer bi-ensemble, plotted as functions of site-occupation of the first site for various weights. We set $U = 1$ in the left, $U = 5$ in the center, and $U = 10$ in the right.

Looking at Figs. S8 and S9, one can see that the correlation inequalities of Eq. 13 are satisfied for all values of Δn_w. As noted in the main text, there exists a clear trend with respect to weight for the symmetric dimer, with the ground-state having the maximum magnitude in each plot, and decreasing in magnitude with w. This trend no longer holds for any nonzero value of Δn_w. Alternative approaches were implemented in which Δv was held fixed, again showing no clear trend for asymmetric dimers. Furthermore, it is clear that the inequalities of Eq. 13 become equalities as $\Delta n_w \to 2\overline{w}$, explaining the flat behavior of the $w = 0.5$ curves for $\Delta n_w = 1$. It also appears that increasing U morphs the shape of each curve, breaking symmetry around $\lambda = 0.5$ for E_c and U_c.

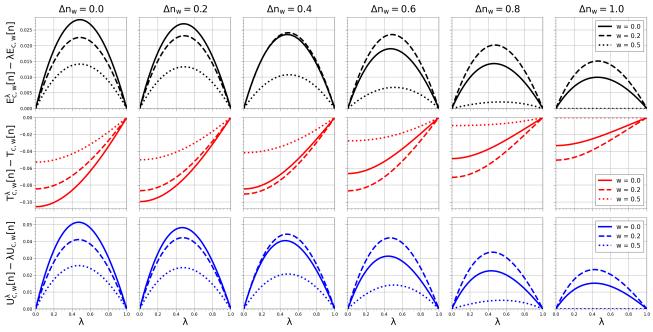

FIG. S8. Correlation inequalities (Eq. 21) for the total (top), kinetic (middle), and potential (bottom) correlation energies, depicted by varying λ in the Hubbard dimer bi-ensemble with $U = 1$.

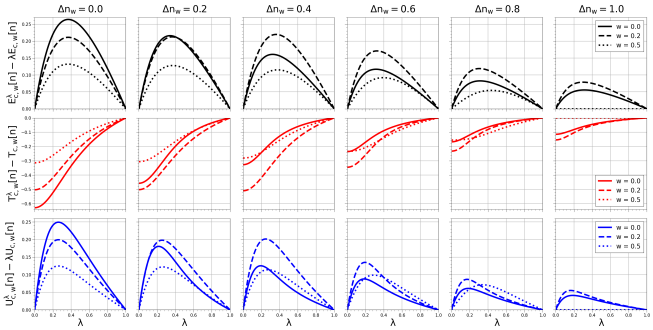

FIG. S9. Correlation inequalities (Eq. 21) for the total (top), kinetic (middle), and potential (bottom) correlation energies, depicted by varying λ in the Hubbard dimer bi-ensemble with $U = 5$.

1.4. Adiabatic Connection

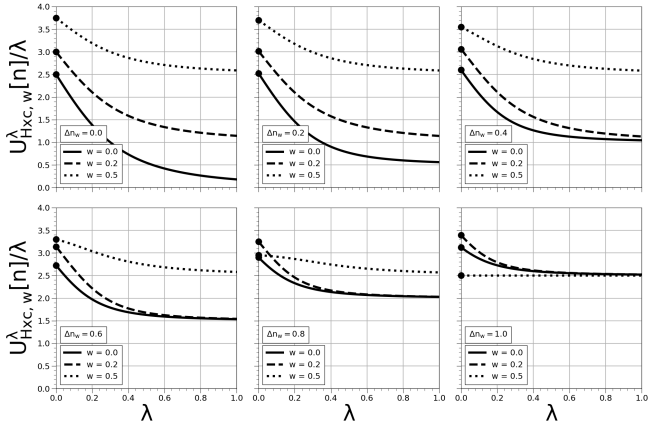

FIG. S10. Ensemble adiabatic connection for $U = 5$ and various Δn_w; circles represent the weight-dependent HX energy, which the HXC expression approaches as $\lambda \to 0$.

In this section we include plots depicting more adiabatic connection curves than just that of Fig. 3 of the main text.

We first note that all curves of a given weight look similar to ground-state DFT curves. They are monotonically decreasing and are convex. Looking at Fig. S10 one can observe an interesting change in ordering of the HX energy values based on the weights. For $\Delta n_w < 0.6$ the HX energy monotonicly decreases in value as the weights increase and the spacing between the values shrinks. However, after that point the ordering shifts and the $w = 0.5$ weight has the maximum HX value. Additionally, as the $\Delta n_w \to 1$ the asymptotic value of the HXC expression is same for all weights.

2. STRONG CORRELATION LIMITS OF ENERGY COMPONENTS

2.1. Large U Expansions

For fixed w, as U becomes large, one can either keep Δv fixed, or $\Delta v/U$ fixed. The former was explored by Deur et al. [4], and produces the pale blue curves of Fig. 5 of the main text. As is clear from the figure, the blue curves yield the correct answer only for $|\Delta n_w| \leq 2w$, which shrinks to a point as $w \to 0$.

The appropriate expansion to find $E_{c,w}(\Delta n)$ for large U is a different one. We take $U \to \infty$, but keep $\Delta v/U$ fixed. This must be done to include values of Δn away from $\Delta n \approx 0$, while including all allowed values of Δn. A careful expansion yields the total energy as a function of $x = \Delta v/U$:

$$E_w(x) \to U\left(g_w^{(0)}(x) + \frac{g_w^{(2)}(x)}{U^2} + \dots\right), \tag{S.9}$$

where

$$g_w^{(0)}(x) = \frac{1}{3}\left(2 - (c - \sqrt{3}s)h\right) - \frac{2shw}{\sqrt{3}}, \tag{S.10}$$

and

$$g_w^{(2)}(x) = \frac{1}{2h}\left(\frac{(\alpha-3)s}{\sqrt{3}} - (\alpha+1)c\right) + \frac{1}{h}\left(\alpha c + \sqrt{3}s\right)w, \tag{S.11}$$

where $\alpha = |4x/(x^2-1)|$, $c = \cos(\phi)$, and $s = \sin(\phi)$ with,

$$\phi = \frac{1}{3}\cos^{-1}\left(\frac{3h^2-4}{h^3}\right), \qquad h = \sqrt{3x^2+1}. \tag{S.12}$$

The angle ϕ is positive for all values of x, where it takes its maximal value of $\pi/3$ as $x \to 0$ and minimal value of 0 as $x \to \pm 1$, and in the limit $\phi(x \to \pm\infty) = \pi/6$. Because the angle is constrained to $0 \leq \phi \leq \pi/3$, the sine and cosine must always satisfy $0 \leq c, s \leq \sqrt{3}/2$.

From this we have the corresponding density via the exact expression $\Delta n_w = 2dE_w/d(\Delta v)$,

$$\Delta n_w(x) = 2\left(g_w^{(0)\prime}(x) + \frac{g_w^{(2)\prime}(x)}{U^2} + \dots\right), \tag{S.13}$$

where primes denote derivatives with respect to x. Retaining only zero-order terms yields,

$$g_w^{(0)\prime}(x) = \frac{1}{h}\left(\frac{(\gamma-3x)s}{\sqrt{3}} - (\gamma+x)c\right) + \frac{2}{h}\left(\gamma c + \sqrt{3}xs\right)w, \tag{S.14}$$

with $\gamma = \mathrm{sgn}(x(1-x^2))$. Because the expansion in U is singular near $x = 0$ and $x = \pm 1$, $g_w^{(2)}(x)$ diverges at $|x| = 1$, and even $n_w^{(0)}(x) = 2g_w^{(0)\prime}(x)$ contains discontinuous steps. While formally correct in the limit $U \to \infty$, the exact density cannot have such steps, due to the Hohenberg-Kohn theorems. We therefore smooth Eq. S.14 with exponentials that become infinitely sharp as $U \to \infty$:

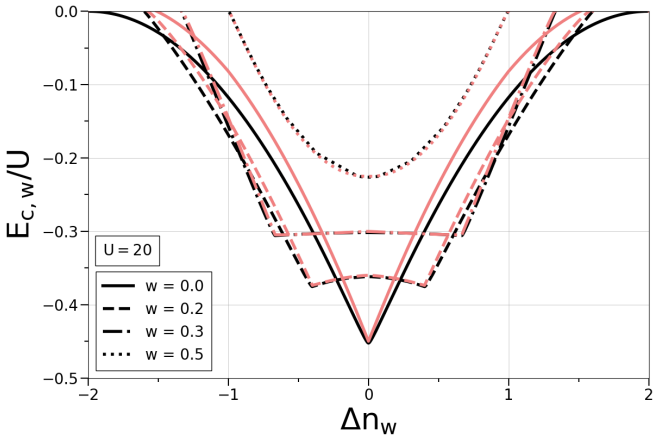

FIG. S11. The exact (black) correlation energy as a function of the exact density and the leading-order expansion in large U (light red) for the correlation energy, using S.10, plotted as a function of the smooth approximation for the density, S.15.

$$\Delta n_w \approx \frac{x}{|x|}(f(|x|)-1)\left(1 + (1-2w)\tanh\left(\frac{\beta(|x|-1)}{2}\right)\right), \tag{S.15}$$

where $f(x) = (\exp(\beta x)+1)^{-1}$ is the Fermi-Dirac distribution with $\beta = 5U$. This is plotted in Fig. S13 and is compared with the exact density. As $U \to \infty$, Eq. S.15 matches Eq. S.14.

Finally we subtract the remaining components to find the correlation energy:

$$E_{c,w}(\Delta n_w(x)) \approx U\left(g_w^{(0)}(x) - \frac{x\Delta n_w(x)}{2} - e_{Hx,w}(\Delta n_w(x))\right) - T_{s,w}(\Delta n_w(x)) + \frac{g_w^{(2)}(x)}{U}, \tag{S.16}$$

where $e_{Hx,w}(\Delta n_w) = E_{Hx,w}(\Delta n_w)/U$. Including only lowest order, and inserting the smooth density, Eq. S.15, yields the plot in figure Fig. S11, and the curves in Fig. 5 of the main text. We also plot the the next order contribution to the correlation energy, Eq. S.16, in Fig. S12. To avoid divergences from α at $x = \pm 1$ we use a smooth approximation to the absolute values that appear in the denominator of Eq. S.11.

2.2. Correlation Energy on the Adiabatic Connection

We produce an expression for $E_{c,w}^{\lambda}(\Delta n_w)$ where Δn_w is kept fixed for each λ along the adiabatic connection. For sufficiently large U we neglect all terms of $O(1/U^2)$ and lower. In this limit, $\Delta n_w(x) \to \Delta n_w^{(0)}(x)$, and by the adiabatic connection construction we have the requirement

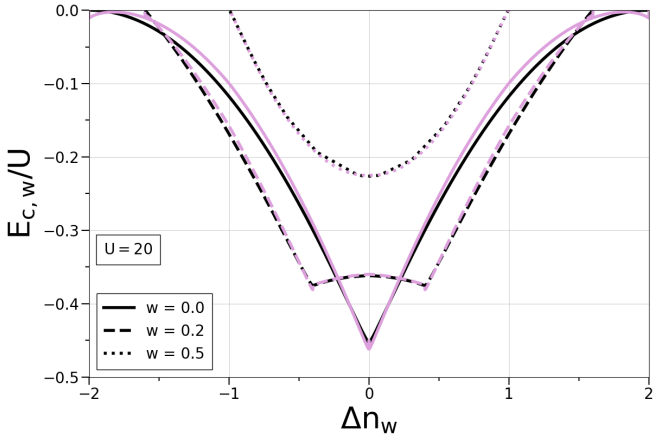

FIG. S12. The exact (black) correlation energy as a function of the exact density and our higher-order expansion in large U (light purple) for the correlation energy, S.16, plotted as a function of the smooth approximation for the density, S.15.

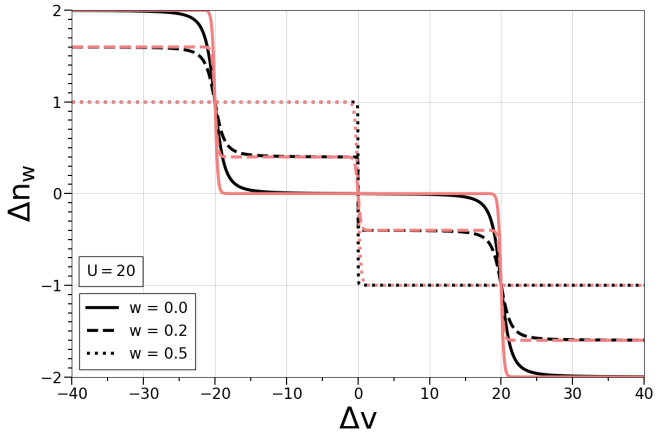

FIG. S13. Smooth approximation for the density S.15 (light red) and the exact density (black) S.3 plotted against Δv.

that $\Delta v/U \approx \Delta v^\lambda/(\lambda U)$, where Δv^λ is the λ-dependent potential that keeps Δn_w fixed along the connection. As a consequence, to leading-order,

$$\Delta v^\lambda(\Delta n_w) \approx \lambda \Delta v^{(0)}(\Delta n_w), \tag{S.17}$$

and thus,

$$E_w^\lambda(\Delta n_w) \approx \lambda U g_w^{(0)}(x^{(0)}(\Delta n_w)) + \frac{g_w^{(2)}(x^{(0)}(\Delta n_w))}{\lambda U}, \tag{S.18}$$

where $x^{(0)}(\Delta n_w) = \Delta v^{(0)}(\Delta n_w)/U$ is the inversion of the leading-order density-potential map Eq. S.17. To produce the correlation energy we subtract from Eq. S.18 the external potential energy (along the connection curve), the KS kinetic energy Eq. S.4, and the HX energy Eq. S.5,

$$E_{c,w}^\lambda(\Delta n_w) \approx \lambda U\Big(g_w^{(0)}(x^{(0)}(\Delta n_w)) - \frac{x^{(0)}(\Delta n_w)\Delta n_w}{2} - e_{Hx,w}(\Delta n_w)\Big) - T_{s,w}(\Delta n_w) + \frac{g_w^{(2)}(x^{(0)}(\Delta n_w))}{\lambda U}, \tag{S.19}$$

where Δn_w remains fixed for all λ.

2.3. Contributions to the Energy

Equation 20 of the main text yields expressions for the separate kinetic and potential contributions to the correlation energy,

$$T_{c,w}(\Delta n_w) \approx \frac{2g_w^{(2)}(x^{(0)}(\Delta n_w))}{U} - T_{s,w}(\Delta n_w), \tag{S.20}$$

$$U_{c,w}(\Delta n_w) \approx U\Big(g_w^{(0)}(x^{(0)}(\Delta n_w)) - \frac{x^{(0)}(\Delta n_w)\Delta n_w}{2} - e_{Hx,w}(\Delta n_w)\Big) - \frac{g_w^{(2)}(x^{(0)}(\Delta n_w))}{U}. \tag{S.21}$$

From the separate contributions of the correlation energy we deduce that,

$$T_w(\Delta n_w) \approx \frac{2g_w^{(2)}(x^{(0)}(\Delta n_w))}{U}, \tag{S.22}$$

$$V_{ee,w}(\Delta n_w) \approx U\left(g_w^{(0)}(x^{(0)}(\Delta n_w)) - \frac{x^{(0)}(\Delta n_w)\Delta n_w}{2}\right) - \frac{g_w^{(2)}(x^{(0)}(\Delta n_w))}{U}. \tag{S.23}$$

We plot Eqs. S.20-S.23 in Fig. S14 with the exact expressions in black and the approximate expressions evaluated with the smooth density in purple. In all plots we use the same smooth approximation to the absolute values in the denominators of $g_w^{(2)}(x)$, Eq. S.11. There are errors in the plots of the correlation kinetic energy, but these vanish as $U \to \infty$.

We compare our result in Eq. S.16, for $|\Delta n_w| \le 2w$, with the symmetric limit expansion of Deur et al. [4]. To properly compare our approximate correlation energy to the previously reported expansion in the symmetric limit, we produce the weight-dependent constant that vanishes in the limit $U \to \infty$,

$$\frac{E_{c,w}(\Delta n_w)}{U} \approx \frac{\overline{w}}{U} - \frac{1}{2}\left(\overline{w} - \frac{(3w-1)}{\overline{w}^2}\frac{\Delta n_w^2}{4}\right), \tag{S.24}$$

which is derived following the procedure in Ref [4]. In Fig. 5 of the main text we plot our approximate leading-order correlation energy Eq. S.16 evaluated with smooth density along with Eq. S.24.

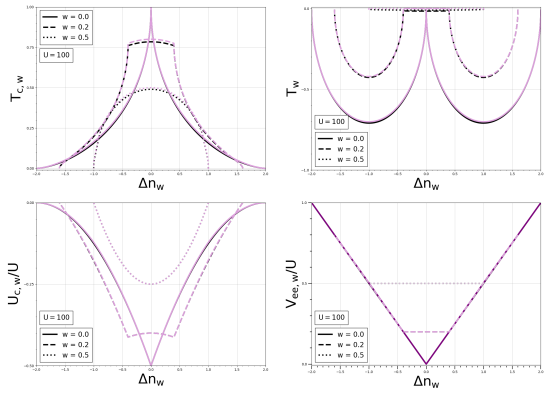

FIG. S14. $T_{c,w}$ (S.20), $U_{c,w}$ (S.21), T_w (S.22), and $V_{\mathrm{ee},w}$ (S.23) for various values of w and $U = 100$. The exact values in the strongly correlated limit are represented by the black curves, which are exact as $U \to \infty$.

3. ENSEMBLE HARTREE-FOCK APPROXIMATION

We now turn our attention to the ensemble generalization of Hartree-Fock. We define the Hartree-Fock solution of each state (analogous to Eq. S.2) to be

$$|\Phi_i\rangle = \alpha_i^{\mathrm{HF}}\left(|12\rangle + |21\rangle\right) + \beta_i^{+\mathrm{HF}}|11\rangle + \beta_i^{-\mathrm{HF}}|22\rangle\,, \qquad \text{(S.25)}$$

with coefficients determined to first order in U:

$$\alpha_0^{\mathrm{HF}} = 2t/c_0^{\mathrm{HF}} \qquad \alpha_1^{\mathrm{HF}} = -\Delta v_{\mathrm{eff},w}^2/2tc_1^{\mathrm{HF}}$$
$$\beta_0^{\pm\mathrm{HF}} = 1/2 \pm \Delta v_{\mathrm{eff},w}/c_0^{\mathrm{HF}} \qquad \beta_1^{\pm\mathrm{HF}} = \pm\Delta v_{\mathrm{eff},w}/c_1^{\mathrm{HF}}$$
$$c_0^{\mathrm{HF}} = 2\sqrt{4t^2 + \Delta v_{\mathrm{eff},w}^2} \qquad c_1^{\mathrm{HF}} = \Delta v_{\mathrm{eff},w}\sqrt{2 + \Delta v_{\mathrm{eff},w}^2/2t^2}$$

Here the weight-dependent effective mean-field potential $\Delta v_{\mathrm{eff},w}$ takes the form [4]

$$\Delta v_{\mathrm{eff},w} = \Delta v + \frac{(1-3w)}{\overline{w}^2}\frac{U\Delta n_w^{\mathrm{HF}}}{2} \qquad \text{(S.26)}$$

where Δn_w^{HF} is found from (S.3) with coefficients as above.

3.1. Densities and Total Energy

The self-consistent EHF density is found numerically throughout this work by solving (S.26). Plots of the exact/EHF self-consistent site-occupation differences are included below in Fig. S15 for various interaction strengths, $U = 0,\ 1,\ \&\ 5$. Here (and for the remainder of this section) we denote the exact solution using solid curves, and the EHF approximation using dashed curves. Looking at the left panel ($U = 0$) of Fig. S15, the EHF approximation matches the exact density exactly, as expected in the limit of weak correlation. One can see that the exact/EHF densities (regardless of weight) begin to differ as U is increased, but must always match at the origin (where $\Delta v = \Delta n_w = 0$) and as $\Delta v \to \infty$ (where $|\Delta n_w| = 2\overline{w}$). This behavior would be expected to hold for larger U values, although as noted previously in Ref. 4, there exists a critical interaction strength U_{crit} at which nonphysical behavior is observed for symmetric dimers with bi-ensemble weight $w \geq 1/3$. This critical interaction strength is

$$U_{\mathrm{crit}} = \frac{\overline{w}}{3w-1}. \qquad \text{(S.27)}$$

For $w \to \frac{1}{2}$, $U_{\mathrm{crit}} \to 1$. At this point the energy expression for dimers with $U > U_{\mathrm{crit}}$ have multiple degenerate minima. This explains the deviation from expected behavior for $w = 0.4,\ 0.5$ in the right panel of Fig. S15, where both curves approach a finite value as $\Delta v \to 0$.

We also plot the exact/EHF bi-ensemble total energy below, using two interaction strengths ($U = 1$ and $U = 5$) to examine the EHF approximation in more detail. We depict this quantity as a function of Δv below in Fig. S16 and separate each w value in new plots to better illustrate the weight-dependence of E_w and E_w^{HF}.

Analyzing Fig. S16, one can see that the EHF approximation obeys the variational principle for all viable weight values (where $w \leq 0.5$); as the weight of the first-excited state is increased, both the exact/EHF energy becomes more positive for all Δv. We note that the EHF approximation always approaches the exact energy as $\Delta v \to \infty$, as shown previously for the ground state. [5]

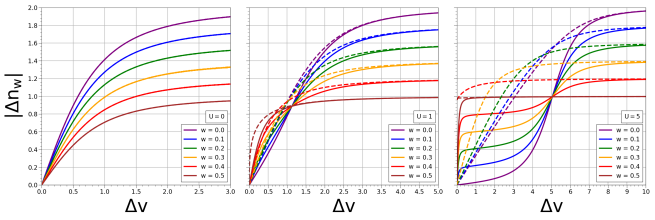

FIG. S15. Absolute value of the density of the Hubbard dimer bi-ensemble, plotted for various weight values as a function of Δv. Here we set $U = 0$ (left), $U = 1$ (center), and $U = 5$ (right). Dashed curves represent the ensemble HF approximation, and the solid curves are exact.

3.2. Correlation Energy

Below we provide plots of the total weight-dependent correlation energy, as well as its kinetic/potential contributions, in Figs. S17, S18, and S19. Note that the definition of the EHF correlation energy is

$$E_{\mathrm{c},w}^{\mathrm{HF}} = E_w[n_w] - E_w^{\mathrm{HF}}[n_w^{\mathrm{HF}}], \qquad \text{(S.28)}$$

where each energy functional has been minimized by its respective weight-dependent self-consistent density.

Looking at Fig. S17, it is evident that the behavior of the correlation energy greatly depends upon the value of w. We find that the inequality relating the exact/approximate correlation energy holds for all ensembles (i.e. $E_{\mathrm{c}}^{\mathrm{HF}} \geq E_{\mathrm{c}}$ for all weights). We show that a different trend exists for the kinetic/potential correlation components, as the inequalities describing the ground state ($T_{\mathrm{c}}^{\mathrm{HF}} \leq T_{\mathrm{c}}$ and $U_{\mathrm{c}}^{\mathrm{HF}} \leq U_{\mathrm{c}}$) no longer apply for ensembles with $w \neq 0$.

Note that for each of these quantities, the EHF approximate correlation energy matches the exact solution at $\Delta v = 0$, except for strongly correlated systems with $w \geq 1/3$ (due to the nonphysical behavior in this regime discussed previously).

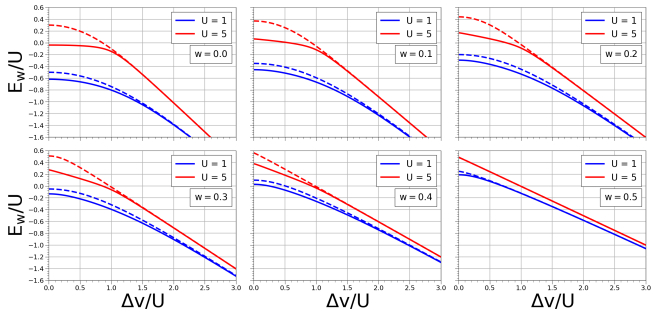

FIG. S16. Total energy of the Hubbard dimer bi-ensemble plotted as a function of Δv for various w values. Dashed lines are the HF approximation and the solid lines are exact.

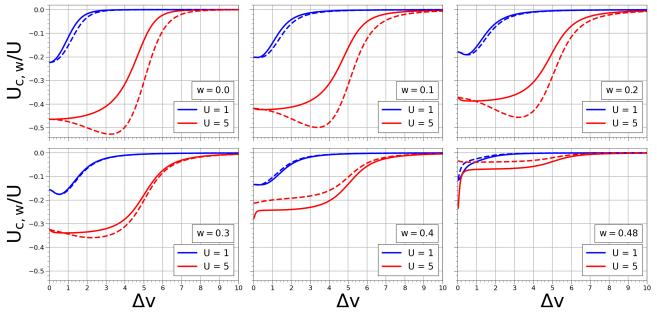

FIG. S19. Potential correlation energy of the Hubbard dimer bi-ensemble plotted as a function of Δv for various w values. Dashed lines are the HF approximation and the solid lines are exact.

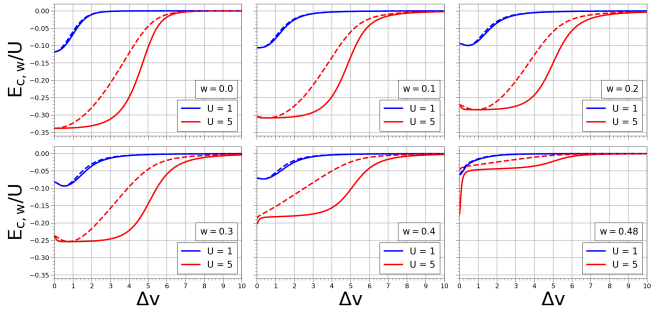

FIG. S17. Total correlation energy of the Hubbard dimer bi-ensemble plotted as a function of Δv for various w values. Dashed lines are the HF approximation and the solid lines are exact.

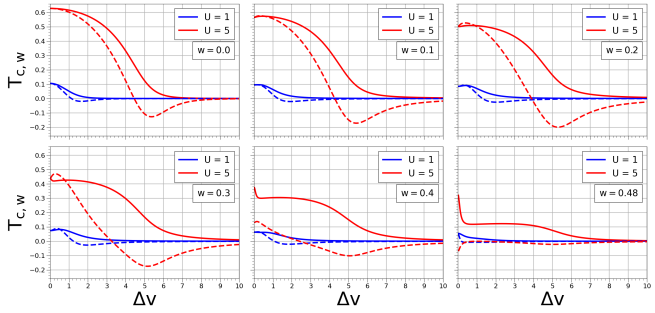

FIG. S18. Kinetic correlation energy of the Hubbard dimer bi-ensemble plotted as a function of Δv for various w values. Dashed lines are the HF approximation and the solid lines are exact.

[1] K. Deur, L. Mazouin, and E. Fromager, Phys. Rev. B **95**, 035120 (2017).
[2] J. C. Smith, A. Pribram-Jones, and K. Burke, Phys. Rev. B **93**, 245131 (2016).
[3] A. Pribram-Jones, Z.-h. Yang, J. R. Trail, K. Burke, R. J. Needs, and C. A. Ullrich, J. Chem. Phys. **140**, 18A541 (2014).
[4] K. Deur, L. Mazouin, B. Senjean, and E. Fromager, The European Physical Journal B **91**, 1 (2018).
[5] D. J. Carrascal, J. Ferrer, J. C. Smith, and K. Burke, Journal of Physics: Condensed Matter **27**, 393001 (2015).